Bulletin of the Seismological Society of America, 89, 3, pp. 785–795, June 1999

Recent Earthquake Sequences at Coso: Evidence for Conjugate Faulting and Stress Loading near a Geothermal Field

by Joydeep Bhattacharyya, Susanna Gross, Jonathan Lees, and Mike Hastings

Abstract Two recent earthquake sequences near the Coso geothermal field show clear evidence of faulting along conjugate planes. We present results from analyzing an earthquake sequence occurring in 1998 and compare it with a similar sequence that occurred in 1996. The two sequences followed mainshocks that occurred on 27 November 1996 and 6 March 1998. Both mainshocks ruptured approximately colocated regions of the same fault system. Following a comparison with the background seismicity of the Coso region, we have detected evidence of stress loading within the geothermal field that appears to be in response to the 1998 earthquakes. The M_L = 5.2 mainshock in the 1998 sequence occurred at 5:47 a.m. UTC and was located approximately 45 km north of the town of Ridgecrest in the Coso range. The mainshock of the 1996 sequence had an M_L magnitude of 5.3. There have been no observable surface ruptures associated with either of these sequences. Though the mainshocks for both sequences were located about 900 m apart and have nearly the same local magnitudes, the sequences differ in both their temporal and spatial characteristics. An analysis of the fault-plane solutions of the mainshocks and the aftershock locations suggests that the two sequences ruptured fault planes that are perpendicular to one another. We observe a much faster temporal decay of the 1998 sequence compared to the one in 1996; moreover, while the 1996 sequence was not followed by any sizeable (i.e., $M_L > 4.0$) aftershocks, the 1998 sequence had four such events. From an estimate of the tectonic stressing rate on the fault that produced the 1998 sequence, we infer a repeat cycle of 135 years for an earthquake of comparable magnitude at Coso.

Introduction

The Coso earthquake sequence of 1998 started with the mainshock on 6 March 1998 (Fig. 1a). The mainshock had a hypocentral location within 900 m of an event of comparable size that occurred on 27 November 1996. We will refer to the earthquakes as Eq98 and Eq96, respectively. The two earthquakes share some common features. The location of their hypocenters are within the Coso range, and both produced significant aftershock sequences. The earthquakes in both sequences occurred in a region located in the Owens valley, flanked by the Sierra Nevada frontal fault system to the west, the Argus range to the east and south, the Indian Wells valley to the south, and the Inyo mountains to the north. As expected for this region in California, north- to NNE-trending normal faults are dominantly observed in much of the Coso range (Duffield *et al.*, 1980).

In the past, local earthquake data have been used extensively to constrain the tectonic setting of the Coso region (Combs and Rotstein, 1976; Walter and Weaver, 1980; Roquemore, 1980, 1987; Malin, 1994; Feng and Lees, 1998; Wu and Lees, 1996, 1999). The Coso area is an active microearthquake zone primarily because of the presence of the nearby geothermal field. Much of the seismicity inside the geothermal field can be linked to the injection of fluids inside the field (Malin, 1994; Lees, 1998). On a regional scale, the earthquake sequences occurred in the eastern California shear zone, ECSZ (Hauksson *et al.*, 1995). Although ECSZ is characterized by several large earthquakes (for example, the 1992, M = 7.3, Landers earthquake and the 1872, M = 8.0, Owens valley earthquake), large earthquakes in the immediate vicinity of Eq96 and Eq98 are rare. The largest earthquake recorded near the Coso Range was the 1946 Walker Pass earthquake of M = 6.3 located about 40 km southwest of Coso Hot Springs (Southern California Earthquake Catalog, Wald *et al.*, 1997). In their analysis of local earthquakes, Walter and Weaver (1980) pointed out that the Coso range is largely characterized by diffuse earthquake activity with an approximate northwest-striking trend; however, the only seismic activity the authors reported in the part of the Coso range where EQ96 and EQ98 occurred is episodic and gives rise to significant aftershock sequences,

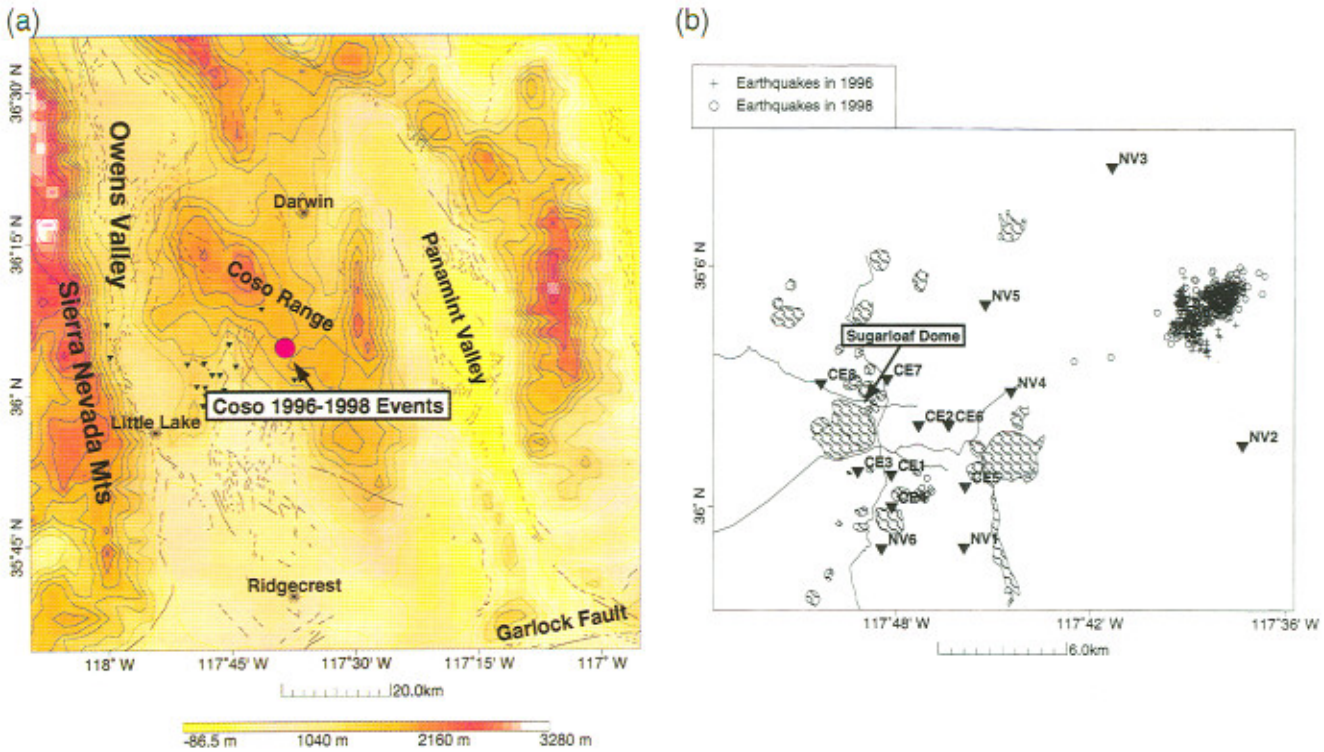

Figure 1. Map of the study area showing the major faults and the earthquake locations. (a) Elevation map of the Coso region. The mainshock locations that give rise to the aftershock sequences analyzed in this study are shown in the context of the regional geology of eastern California. In the scale of the map, both the events have nearly identical locations. The fault locations, shown in the plot as black lines, are from Jennings (1994). The locations of the seismic stations in the Coso microearthquake network (MEQ) are shown by solid triangles. (b) The 1996 and 1998 earthquake sequences that have been analyzed in this study. They have been relocated using the Coso velocity model of Wu and Lees (1998) using waveforms recorded in the MEQ network. For the 1998 events, we only show the aftershocks that occurred within a week of the mainshock. The errors in the earthquake locations are ≈500 m. We note the nearly perpendicular trends between the two sequences. The locations and names of the MEQ stations are shown by the solid triangles. The shaded regions indicate the rhyolite domes observed close to the geothermal field.

some of which have been shown to last for more than a year. These sequences typically originate with a magnitude 4 to 5 earthquake and are followed by a few thousand smaller events. One of the sequences reported by Walter and Weaver (1980) (named D), is located just east of the EQ96 and EQ98 sequences. The trend of the aftershock activity and the preferred focal mechanism suggest left-lateral strike-slip faulting on a NE-striking fault plane produced D.

The mainshocks of the sequences in 1996 and 1998 show some similar features. They had similar magnitudes, that is, 5.3 for Eq96 and 5.2 for Eq98, that occurred within 900 m of one another in a region where large earthquakes are rare and the two fault plane solutions (Table 1; Douglas Dreger, personal comm.) are nearly identical. Hence, Eq96 and Eq98 probably ruptured colocated patches of the same fault system.

The question then arises whether Eq98 reactivated the fault ruptured by Eq96. The spatial and temporal distribution of the aftershocks, which give us estimates of the direction and extent of rupture of the faults, can be used to address this question (e.g., Hauksson *et al.*, 1995; Thomas *et al.*, 1996). Using seismic waveforms recorded in a nearby network of three-component, short-period, high-dynamic range, borehole seismometers inside the geothermal field [Fig. 1b and described in Alvarez (1992) and Wu and Lees (1996)], we can accurately determine earthquake locations. Using a stress estimation technique (Gross, 1996; Gross and Kisslinger, 1997), we have estimated the change in failure stress inside the geothermal field due to Eq98. Finally, the change in failure stress is used to compute the stress rate with which we estimate a recurrence interval for an earthquake of similar magnitude that ruptures the fault that produced Eq98.

In the following sections, we describe and compare the important features of the two earthquake sequences and estimate stress changes at Coso produced by the 1998 earthquake sequences.

Table 1
Source Mechanisms of the Larger Coso Earthquakes of 1996 and 1998

Event Day	Event Time (UTC) (Hour:Min:Sec)	Focal Plane 1			Focal Plane 2		
		Strike (°)	Dip (°)	Rake (°)	Strike (°)	Dip (°)	Rake (°)
27 November 1996	20:17:23.59	333	81	−177	242	87	−9
6 March 1998	5:47:39.71	233	87	−13	324	77	−177
6 March 1998	5:49:43.17	247	88	−8	337	82	−178
6 March 1998	5:54:21.14	254	82	20	341	70	172
6 March 1998	0:36:46.29	250	89	−15	340	75	−179

Note: The source mechanisms have been obtained from Douglas Dreger.

The Earthquake Sequence of 1998

Mainshock

The mainshock of the 1998 sequence was an $M_L = 5.2$ earthquake that occurred on 6 March at 5:47:39.71 UTC. The earthquake, Eq98, was located in the Coso Range approximately 17 miles ENE of Little Lake and was clearly felt in nearby towns of Ridgecrest and Little Lake (Fig. 1a). EQ98 was the largest event in southern California for more than 1 year. Using the nearby stations of the Coso microearthquake network (MEQ), we relocated the earthquake to 36.0468° N ± 0.2 km and 117.3844° W ± 0.34 km and source depth of 9.77 ± 0.67 km. The earthquake was clearly recorded on 15 MEQ stations with the closest station being about 6 km away. Of these, 11 high-quality waveforms were used for locating the earthquake. The earthquake locations may be slightly biased because the event is outside the main MEQ network, and there is an azimuthal gap of 194° between the source-receiver paths. A reconnaissance geological survey of the aftershock region did not provide any obvious evidence for surface rupture (Frank Monastero, personal comm.).

Aftershock Sequence. We relocated all aftershocks using *P*- and *S*-wave travel times recorded at MEQ. Station corrections were obtained from Wu and Lees (1999) following analysis of a much larger dataset of local earthquakes recorded at these stations. This same dataset was used to compute regional one-dimensional compressional and shear-wave velocity models used for routine relocation. Each of the aftershock locations were obtained independently, and in Figure 2, we show the mainshock and aftershocks leading up to the largest aftershock, Eq98.a, an event of $M_L = 5.0$ (as reported by the Southern California Earthquake Center, SCEC). The mainshock occurred at the deepest point of the sequence at a depth of 9.77 km (Fig. 2b), and the hypocentral locations of the aftershocks had a shallowing trend, striking NNE. We note that there were 3 large aftershocks, of $M_L \geqq 4.0$, immediately following the mainshock. Fault plane solutions for the larger earthquakes in 1998 are provided in Table 1. The solutions are consistent with both body waves and surface waves for the same events recorded at the Southern California Seismic Network, SCSN (Jim Mori, USGS, personal comm.). From the aftershock locations and geometry of the fault plane, we infer that the larger earthquakes of 1998 ($M_L \geqq 4.0$) ruptured along the same fault. From the focal plane solutions of these earthquakes (Table 1), we propose that the rupture surface has a strike of ≈246°. The focal mechanisms indicate a left-lateral strike-slip faulting pattern, consistent with earthquakes in the nearby Darwin Wash region of the Coso range (Walter and Weaver, 1980). A recent geological study suggests that a strike-slip fault is present in the region of the aftershocks at depth (Whitmarsh, 1998); a surface expression of the fault, however, has not been documented.

The largest aftershock in the 1998 sequence is an event with magnitude $M_L = 5.0$ (Eq98.a). The Eq98.a event (Fig. 3) occurred on 7 March 1998 at 00:36:46.29 UTC. We show only events that occurred within 24 hours following this large aftershock. Event Eq98.a was located at 36.054° N latitude and 117.3701° W longitude, at a depth of 7.72 km with magnitude and rupture direction similar to that of the mainshock, Eq98 (Table 1). Event Eq98.a approximately marks the easternmost end of the aftershock sequence, and subsequent events occurred toward the geothermal field. We conclude that Eq98.a most probably marks a transition in the faulting process and suggests a reversal in rupture direction. The surface projection of Eq98.a is close to the expected boundary between the NNE-trending fault along which rupture occurs and a NW-trending fault (Whitmarsh, 1998). We hypothesize that the latter fault probably stopped the northeast-trending rupture process; from Figures 3b, however, we infer that Eq98 and Eq98.a approximately mark the spatial limits of the rupture.

Temporal Decay of the Aftershock Sequence. The temporal decay of aftershock sequences can be used to obtain information about mechanisms of stress relaxation and physical processes of source regions (Mikumo and Miyatake, 1979; Dieterich, 1986, 1994). Temporal decay is usually obtained from fitting empirical relations to the earthquake data (Kisslinger and Jones, 1991; Gross and Kisslinger, 1994). The modified Omori model, MOM (Utsu, 1961), is the model most commonly used by seismologists and can be considered a standard to which other aftershock decay relations may be compared (Kisslinger, 1996). A re-

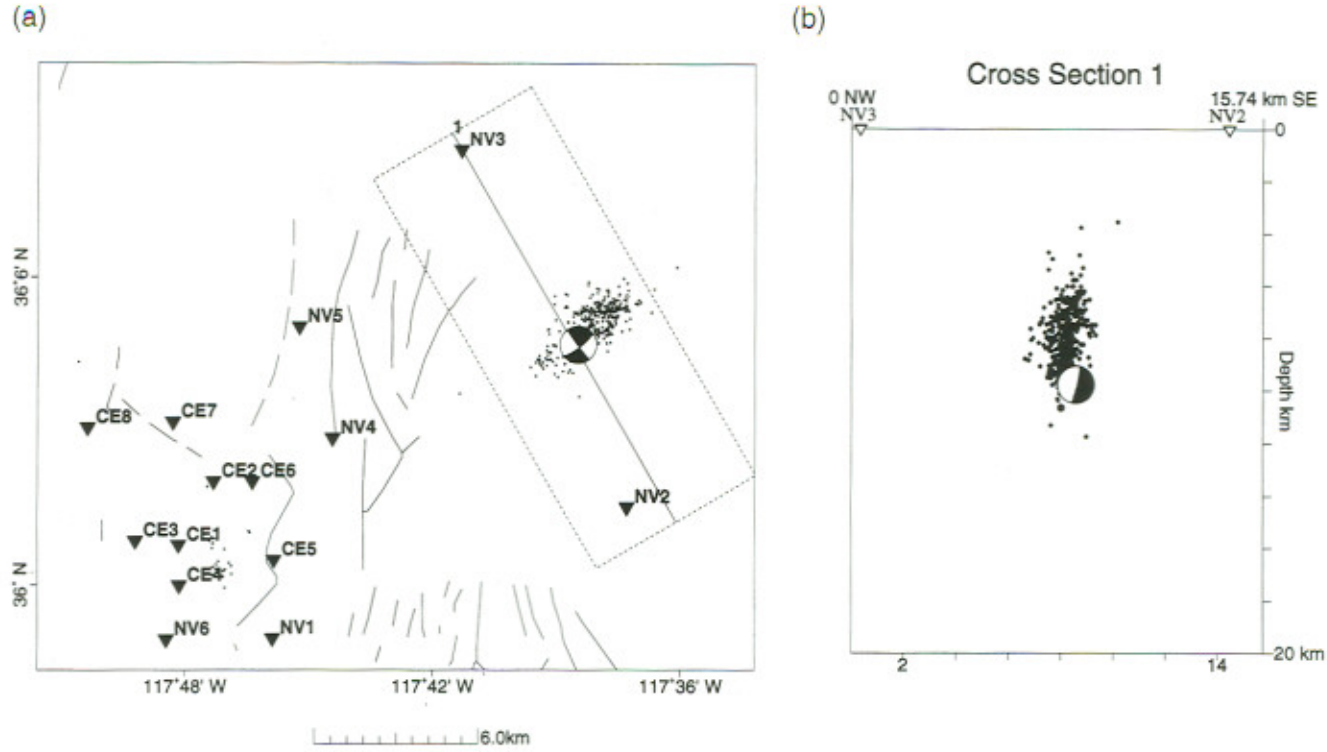

Figure 2. Locations of earthquakes occurring in the first day of the 1998 sequence. (a) The locations in map view along with the source mechanism of the mainshock, Eq98, is also shown (Table 1). The aftershocks follow a trend that is nearly coincident with one of the nodal planes of the source. We infer that this plane defines the rupture surface for these events. (b) Cross section perpendicular to the rupture surface of the 1998 events (mentioned as 1 in part a). The source mechanism of the mainshock is shown that indicates a nearly pure strike-slip motion. Note that the mainshock occurs at the bottom of the earthquake sequence.

cently proposed stretched exponential model, SEM (Kisslinger, 1993), has been shown, in certain cases, to fit data better than MOM. SEM has the advantage that it never produces an infinite number of aftershocks and has a decay time analogous to a half-life, which may be intuitively related to physical processes of decay. We also consider an analytic model of earthquake nucleation presented by Dieterich (1994) that can be used to calculate the rate function of earthquake occurrence and draw meaningful physical conclusions about the aftershock process. We have tested the above-mentioned models by fitting them to the temporal decay of the earthquakes (Gross and Kisslinger, 1994). Using a downhill simplex technique, we find the best-fitting model parameters in each case (Gross, 1996). Using the relocation scheme for Coso, we have a dataset of earthquake locations for a duration of 429 days prior to Eq98 (1/1/97 to 3/5/98) and for a 41-day period into its aftershock sequence (3/6-98 to 4/15/98). The rate of daily seismicity at the end of the aftershock sequence approaches the background level experienced by the region close to the Coso geothermal field, that is, 21 events a day. The final dataset consists of 4572 relocated events. We select from this dataset those with at least five *P*-wave travel-time measurements.

Dieterich (1986) proposed that aftershocks are similar to the background earthquakes that have ruptured earlier due to stress loading from the mainshock. This implies that background seismicity continues during an aftershock sequence as a distinct phenomenon. To ascertain the effect of background seismicity on aftershock decay, along with the above-mentioned empirical forms, we also allow fits to models that include the rate of background seismicity. In short, we fit parametric models, with and without a background seismicity rate, to the aftershock decay and compare the fit to the data (Fig. 4). We find that the best-fitting models to the aftershock sequence require a background rate, implying that background seismicity persists during the aftershock sequence (Fig. 4a).

We use the AIC test of Akaike (1974) to estimate the fits of the different seismicity models of aftershock decay to the events in 1998. The SEM model has an AIC value that is larger than the corresponding value for MOM by ≈16. This suggests that the SEM model fits the data significantly better than the MOM model, though both the models misfit the secondary surge of activity (Fig. 4a). For the best-fitting MOM, the most noteworthy feature of the aftershock sequence is the relatively high decay rate with p values larger

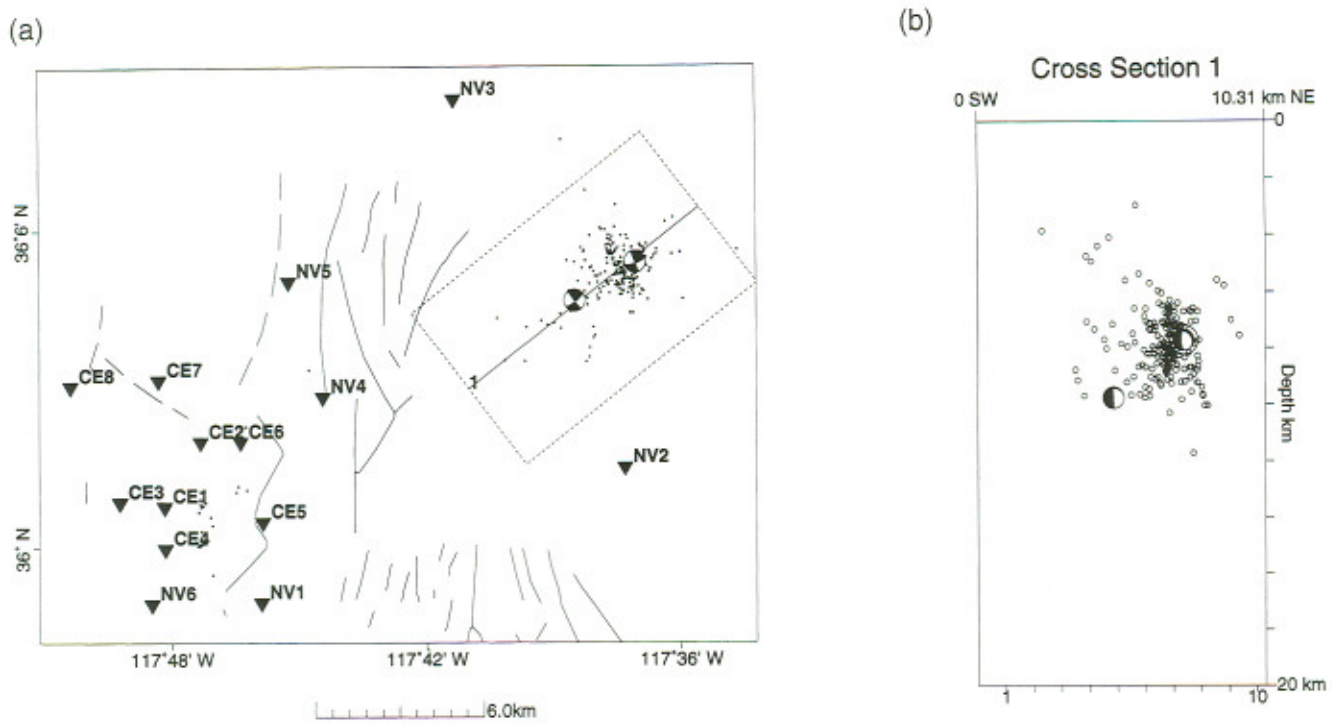

Figure 3. The aftershocks recorded for a day following the largest aftershock of the 1998 sequence. (a) The map view of the locations along with the focal mechanism of the mainshock and this largest aftershock. Note that the focal mechanisms are similar and one of the nodal planes are roughly parallel to the trend of the aftershocks. A comparison with Figure 2a indicates that these two earthquakes approximately define the limits of the seismogenic zone. (b) A cross section along the trend of the aftershocks with the largest events bounding the northeast and southwest ends of the aftershock locations.

than 3. This estimate of p value is not well constrained and is appreciably higher than the average ≈1.1 obtained for California (Reasenberg and Jones, 1989; Kisslinger and Jones, 1991). One explanation for high temporal decay is the presence of unusually high temperatures in the seismogenic zone. Recent studies by Kisslinger and Jones (1991) and Creamer (1994) related high surface heat flow (used as a surrogate for temperature near the hypocenter) in regions of southern California and Japan where earthquake sequences with high decay rates. As proposed by Mogi (1967), the decay rate can be high because of rapid relaxation of residual stress due to heat flow. This hypothesis is reasonable for these Coso events that are close to a geothermal field.

Using earthquake M_L magnitudes (SCEC catalog), we calculate b-values for earthquakes occurring within 1 day after Eq98. The b-values vary slightly with magnitude cutoff: For M_L cutoff values between 1.2 and 2.8, we find that the average b-value is equal to 0.83 ± 0.1.

Stress Changes in the Coso Geothermal Field

The earthquake sequence following Eq98 occurred close to one of the largest active geothermal fields in the world. Several recent studies reported evidence for triggering of earthquakes following the Landers events in southern California (Hill *et al.*, 1993; Bodin and Gomberg, 1994; Anderson *et al.*, 1994). Hill *et al.* (1993) suggested that triggering of aftershocks is more intense in regions of high surface heat flow. These remotely triggered earthquakes are probably due to stress loading of the region by nearby earthquakes coupled with elevated pore pressures due to the presence of geothermal fluids (Hill *et al.*, 1993). Since the Coso geothermal field is in active production, a similar stress loading, if observed, would be of particular interest. Historically, due to the paucity of high-quality seismic stations, most reports of triggered earthquakes involved observations of a rare, large ($M \approx 7.0$) earthquake observed a few hundred kilometers away (Hill *et al.*, 1993). The earthquake sequence near Coso provides the opportunity to investigate seismic triggering in a geothermal field located only a few kilometers away from a more commonly observed $M \approx 5.0$ earthquake. To estimate the static stress loading due to Eq98, we use a simple stress step model (Gross and Kisslinger, 1997; Gross and Bürgmann, 1998). Stress step is defined as the change in static stress at the location of an earthquake produced by a different, nearby event. In our approach, the stress step from the mainshock is used to estimate failure stress, which is a weighted sum of maximum shear and normal stresses (Gross and Bürgmann, 1998). The change in failure stress is

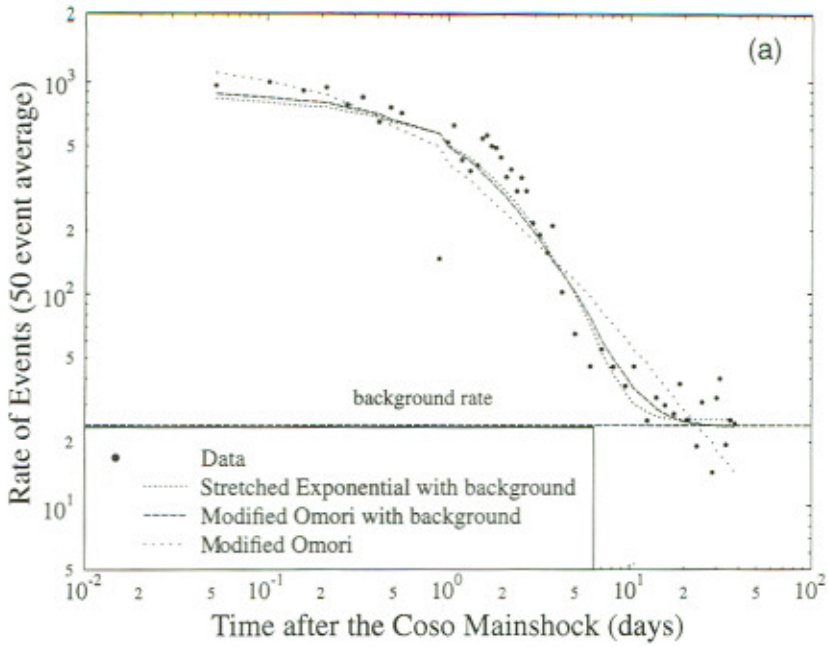

Figure 4. Decay in the number of the 1998 Coso earthquakes as a function of time with three aftershock decay models fit to the data. (a) Fit of the seismicity models to the rate of aftershocks in the 1998 sequence. Models that include a background seismicity rate fit the data better. (b) Fit to the cumulative number of events with the solid line showing the data and the different dashed lines showing the best-fitting models. The background activity is calculated from the rate of earthquakes reported before the mainshock. We choose a 41-day postmainshock window in our analysis, which is longer than the equipartition time for this sequence (please see text). We note that the stretched exponential model (SEM) fits the data better than the modified Omori model (MOM).

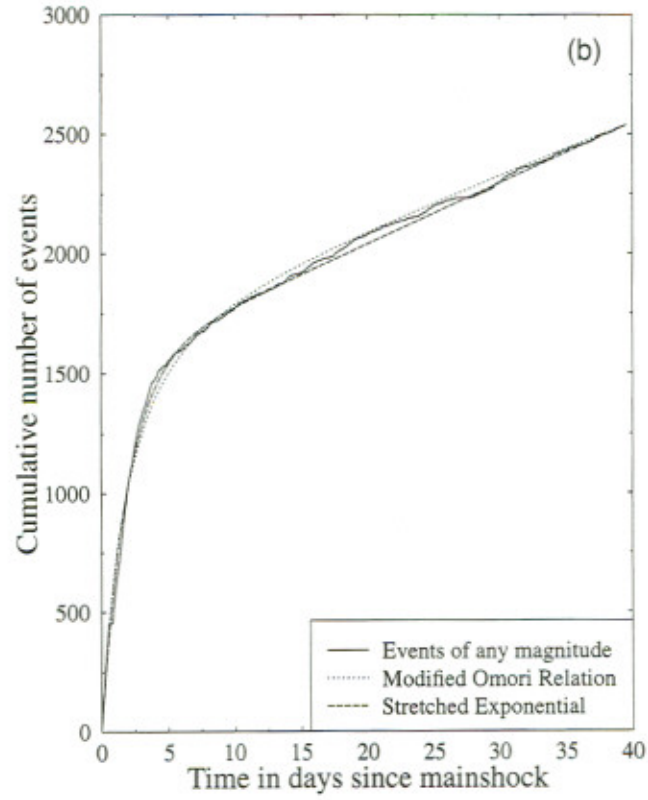

compared to the change in seismicity, as defined by the change in spatial distribution of aftershocks contrasted with background seismicity. The computed failure stresses are largest near the mainshock (Gross and Bürgmann, 1998) where our catalog has consistent seismic monitoring and accurate hypocentral locations. Thus, data from the MEQ network, which had a homogeneous recording before and after the mainshock, is especially suited for stress analysis. The stress estimation technique used in our study makes no assumptions about homogeneous seismic structure, moment release, or statistical independence of the recorded earthquakes. In our technique, we first estimate the effects of the stress step due to the mainshock in the Coso region. The calculated stress step, which is a tensor field, is then compared to changes in observed seismicity at Coso that occur before and after the Eq98 mainshock.

The background seismicity rate was computed from the earthquakes occurring in the region from 1 January 1997 till the onset of Eq98. Since seismicity in the region is relatively homogeneous (Feng and Lees, 1998), the time window used to compute the seismicity can be considered a representative one. We assumed that the background stress state estimated for the seismicity before the Landers earthquake by Hauksson (1994) applied to the nearby Coso area, and we chose a magnitude of background stress (2.2 MPa) and coefficient of friction (0.60) derived from the Landers aftershocks by Gross and Kisslinger (1997). We did not use events from other southern California catalogs in the stress calculations. The computed background seismicity at the equipartition time (Gross and Kisslinger, 1994) is equal to 21 events per day and is consistent with the long-term average activity in the Coso region.

Stress Loading of the Field. We present estimates of the stress changes inside the Coso geothermal field due to the earthquake sequence following Eq98. These stress changes were produced by larger events in the sequence, and therefore, we need to consider their total loading effect. Four events with magnitude greater than 4.0 were combined to create an effective mainshock. It is assumed that these four events ruptured concurrently, so their stress field (a tensoral

quantity) is added to the background stress field to derive the combined total stress field. We now combine the mainshock stress and the background stress to compute the total Coulomb failure stress along optimally oriented planes, σ_F (Reasenberg and Simpson, 1992; King *et al.*, 1994). The failure stress is computed from the principal stresses, σ_i, and the effective coefficient of friction, μ' (Gross and Bürgmann, 1998),

$$\sigma_F = (\sqrt{\mu'^2 + 1}) \left\{ \frac{\sigma_1 - \sigma_3}{2} \right\} + \mu' \frac{\sigma_1 + \sigma_3}{2}. \quad (1)$$

We note that σ_F represents a scalar field. Next, the failure stress for the background stress state is computed. The change in failure stress is estimated by subtracting the two failure stresses, giving a scalar stress step field, $\Delta\sigma_F$. We can thus compute the stress step at the hypocenter locations of events occurring before and after the mainshock. In Figure 5, we show the effect of the stress loading from the mainshock, Eq98. Qualitatively, we observe more areas of stress increase than stress decrease due to the mainshock. To quantify the stress change, the average failure stress inside the Coso geothermal field (defined by [35.98° 36.1°] latitude and [−117.85° −117.5°] longitude) is evaluated for background and aftershock locations. The median stress step for the background and the aftershock events are 1202 and 1305 Pa, respectively. The positive stress step is consistent with the hypothesis that the observed increased Coso seismicity was triggered by the stress step. Significantly, the stress step is larger for the aftershocks compared to the background. This indicates that the stress loading corresponds to a measurable change in the spatial distribution of earthquakes and is responsible for triggering the increased activity inside the field.

Stress Step Modeling. To evaluate the significance of the stress loading near Coso due to Eq98, we need to test how well the change in seismicity correlates with a change in failure stress. We quantify the relationship between the change in stress, that is, the stress step, to the spatial distribution of seismicity by using the **t** statistic (equation 8 in Gross and Kisslinger, 1997),

$$\mathbf{t} = \frac{\overline{\Delta\sigma_F^{\text{before}}} - \overline{\Delta\sigma_F^{\text{after}}}}{\sqrt{s^2_{\text{before}}/N_{\text{before}} + s^2_{\text{after}}/N_{\text{after}}}}, \quad (2)$$

where s is the standard deviation of the stress step values ($\Delta\sigma_F$), N is the number of events in a set of earthquakes, and $\Delta\sigma_F^{\text{after}}$ is the average change in failure stress calculated at the aftershocks. The **t** statistic is similar to cross-correlation where the stress step field is directly compared to seismicity. The **t** statistic is computed for a few spatial bins using two broad time distributions of earthquakes, that is, those occurring before and after the mainshock. The value of the statistic within a bin is roughly the difference in the means of the two distributions normalized by their pooled standard deviations. Moreover, a higher negative value of the statistic indicates a better correlation between stress step and seismicity (Gross and Bürgmann, 1998). For regions within 15 to 25

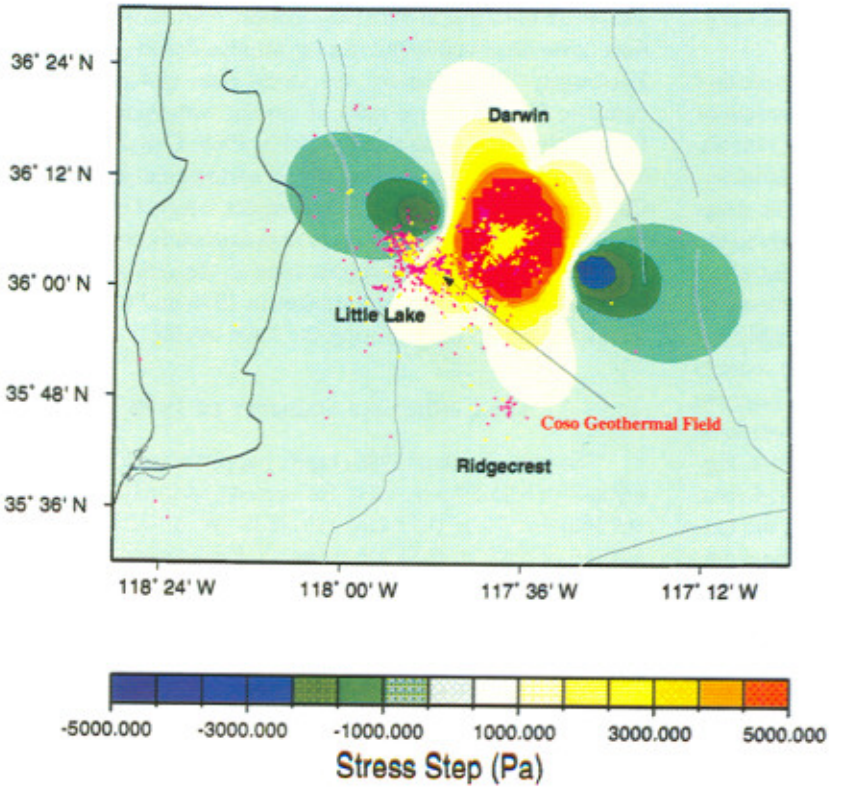

Figure 5. Evaluations of the stress step field in the Coso region produced by the earthquakes in 1998. We show the variations at a depth of 4 km. The events occurring during the sequence of 1998 are shown in yellow, and the hypocenters of the background events are shown in magenta. In the region of the Coso geothermal field, we observe an increase of failure stress, suggesting a stress loading of the field due to the earthquakes. The failure stress indicates that the large earthquakes of 1998 triggers aftershocks inside the geothermal field, which is about 10 km away.

km of Eq98, which encompasses most of the geothermal field, we obtain a value of $\mathbf{t}_2 = -1.5$, whereas for regions within 5 to 15 km of the mainshock, the value of $\mathbf{t}_1 = -21.7$. We infer that an increase in stress step coincides with an increase in seismicity inside the geothermal field, thereby signifying triggering of earthquakes inside the field due to Eq98. For comparison, the value of $\mathbf{t} \equiv \mathbf{t}_1 + \mathbf{t}_2$ is about 5 times smaller than that observed for the Loma Prieta earthquake, summing $\mathbf{t}$ statistics from distance ranges out to 85 km (Gross and Bürgmann, 1998), which is probably related to the smaller Coso mainshock magnitude and catalog. As expected, the correlation is extremely high for events close to the mainshock, indicating that they fit the failure stress model well.

Stress Rate. To estimate the background stress rate, we compute the stress changes from the source model of Eq98 at the hypocenters of the aftershocks for this event and 2574 events representing background activity. We choose events that had at least five *P*-wave picks and divide them into 10 bins so that there are nearly equal number of events in each bin. We first compute the aftershock amplification ratio, the ratio of the aftershock rate $\bar{n}$ to the background seismicity rate r (equation 10, Gross and Bürgmann, 1998),

$$\frac{n_{\text{after}}}{n_{\text{before}}} \frac{1/T_{\text{after}}}{1/T_{\text{before}}} = \frac{\bar{n}}{r}, \tag{3}$$

where n_{before} and n_{after} are the number of events in the background and aftershock periods of durations, T_{before} and T_{after}, respectively. The amplification ratio is then used to compute the stress rate (Gross and Kisslinger, 1997; Gross and Bürgmann, 1998).

The stress rate modeling is based upon the principle that a given stress increment should produce the same amount of seismicity, regardless of how quickly the stress accumulates. The steady tectonic stress creates background seismicity, and the mainshock stress step triggers aftershocks. The stress rate is an important quantity because it relates directly to the seismic hazard of the fault that produced the current aftershock sequence. Our technique requires that estimates of seismicity, source model, and stress state be reasonably accurate. Using stations within a few kilometers of the sources and accurate event locations, as available for Coso, improve the robustness of our technique. We show the variation of the stress step with the aftershock amplification ratio in Figure 6. The error bars on the stress rate are computed from the interquartile range within each bin. In Figure 6, the outlier at high stress step is for a bin located close to the mainshock that, due to slight inaccuracies in the source model, can have wildly varying stress step values. The slope of the line represents the stress rate and is approximately equal to 61 ± 32 Pa/day. The value of the stress rate is comparable to those obtained for Landers and Loma Prieta events using similar techniques [Gross and Kisslinger (1997) Gross and Bürgmann (1998), respectively]. On the other hand, the

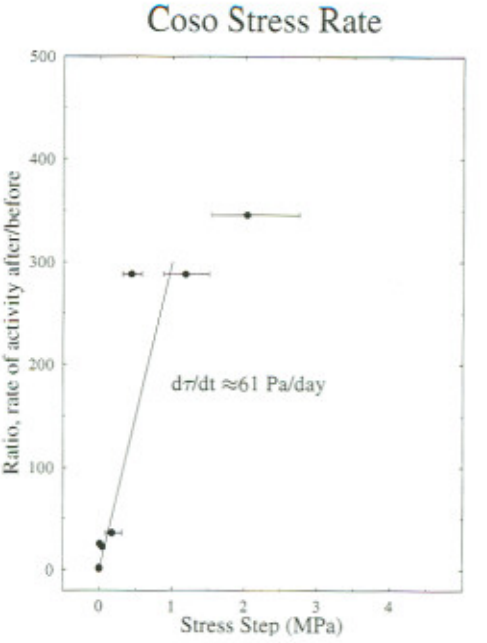

Figure 6. Fits to the aftershock amplification factor as a function of stress step computed for the stress state of the mainshock of the 1998 Coso event, Eq98. The slope s of the straight-line fit to these data can be used to compute stress rate, sigma ≈ $1/(s * T)$, where T is the duration of the aftershock sequence. A straight-line fit gives us the stress rate due to the Eq98 earthquake as equal to 61 ± 32 Pa/day.

stress rate obtained in our study is more than 20 times larger than those observed in the nearby Mojave desert (Gross and Kisslinger, 1997). Finally, the stress rates can be used to compute the recurrence rates of similar earthquakes on the fault that produced the aftershocks in 1998. Considering 3.0 MPa as a typical stress drop for an earthquake in southern California (Scholz, 1990), the recurrence interval in the Coso region is (3.0 MPa/61 Pa/day) or approximately equal to 135 yr. Please note that this repeat time is for rerupturing the fault that produced the earthquakes in 1998 and therefore is distinct from the fault causing the 1996 events.

The Earthquake Sequence of 1996

The mainshock of 1996, Eq96, happened on 27 November at 20:17:23.59 p.m. UTC. Relocated coordinates of Eq96 are 36.0462° N ± 0.53 km, 117.3839° W ± 0.21 km, and a depth of 8.85 ± 0.54 km using 11 *P*-wave and 5 *S*-wave arrival times. The azimuthal gap in the relocation is 249°. As in Eq98, no surface rupture was observed for Eq96. The moment tensor solution for the Eq96 event is given in Table 1 (Douglas Dreger, personal comm.).

We analyzed 135 events in a 49-hr time span following Eq96, with frequent gaps during the last 24 hr. The small number of events is sufficient to roughly define the fault

plane (Fig. 7). Relocated aftershocks show rupture along a northwest-trending fault plane. The NW fault plane is roughly coincident with the strike of the mainshock, Eq96 (Fig. 7), and we infer that the fault plane has a strike of 331°. In Figure 7b, we show aftershock locations along a cross section roughly perpendicular to the strike direction. The aftershock locations suggest that the fault plane has a subvertical dip, approximately equal to the dip of the mainshock, Eq96 (Table 1). The mainshock occurs at the deepest part of the sequence, and the fault is observed to rupture upslip with progressive shallowing of aftershocks. Due to incomplete recording of the 1996 sequence, its rupture surface can be only partially defined.

We used earthquake times and magnitudes, as obtained from the SCEC catalog, to compute the *b*-value and model the temporal decay of the 1996 sequence. There was no single event of $M_L \geqq 4.0$ in the aftershock sequence that followed Eq96. For magnitude cutoffs $\geqq 2.5$, we get *b*-values approximately equal to 1.07 ± 0.02, close to the average southern California value of 1.06 (Kisslinger and Jones, 1991). Furthermore, for the fit to the modified Omori model (Utsu, 1961), the *p* value is equal to 0.8, suggesting a slow aftershock decay. Due to the limited recording of the aftershock sequence by the MEQ network, we have not attempted to compute stress step and stress rate in the geothermal field due to the 1996 aftershocks.

Comparison between the 1996 and the 1998 Earthquakes

The earthquake sequences of 1996 and 1998 occurred less than 10 km away from the Coso geothermal field. Both of these sequences follow mainshocks with $M_L > 5.0$ in a region where large earthquakes are rare (Hauksson *et al.*, 1995). The mainshocks lie about 900 m from one another and can thus be considered to be colocated within the same fault patch. There was no precursory activity to either of these aftershock sequences. Geologic mapping before and after these sequences shows no obvious surface rupture or faults. Aftershocks are all located shallower than mainshocks for each of the sequences. Finally, the focal mechanisms, as given by the principal and the auxiliary planes of the mainshocks, are nearly coincident (Table 1). As expected for Coso, the dip angle for both mechanisms is nearly vertical, suggesting the events occurred along strike-slip faults.

Despite their common locations, the two sequences show distinct differences. The mainshock of 1998 generated stronger aftershocks than that of 1996. The locations of the aftershocks following Eq96 trend along a northwest-striking plane. Aftershocks following Eq98, on the other hand, initially progress in the northeast direction until the occurrence of Eq98.a. Thereafter, aftershocks predominantly occur southwest of Eq98.a, that is, toward the geothermal field.

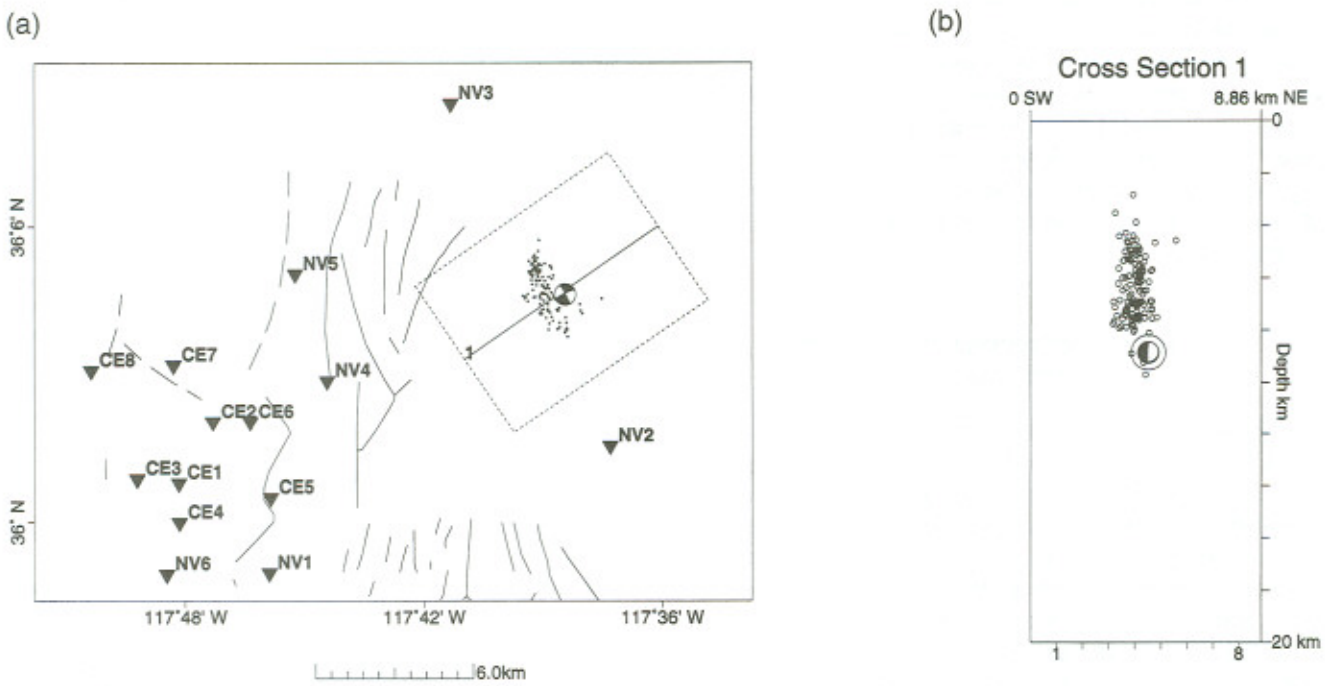

Figure 7. Locations of the earthquakes recorded at MEQ during the 1996 sequence. (a) 135 aftershocks relocated and the source mechanism of the mainshock (Table 1). The aftershock locations along with the source model indicate that the earthquakes are caused by a strike-slip fault rupturing in the northwest direction. (b) Cross section along profile 1 (a) that is roughly perpendicular to the slip direction. We note that the mainshock occurs at the bottom of the rupture with a progressive shallowing of the aftershocks.

Aftershocks of Eq96 and Eq98 thus differ both in their trend and time sequence. From the aftershock locations and mainshock mechanisms, we infer that the ruptures for these sequences occurred along two different faults oriented nearly perpendicular to one another. Finally, we see that the sequences also differ in their distribution of magnitudes. The *b*-values of the 1996 and 1998 sequences are equal to 1.05 and 0.8, respectively, a considerable difference. We observe faster temporal decay for the aftershock sequence of Eq98 compared to that following Eq96.

Evidence for Conjugate Faulting

Eq96 was produced by right-lateral strike-slip faulting on a NW-striking fault plane. This type of faulting dominates in the Coso Range (Roquemore, 1980; Jennings, 1994). Conversely, the 1998 earthquakes occurred along a NE-striking, left-lateral fault system. The proximity of the mainshocks, coupled with the perpendicular relationship between the strike planes, suggests that these earthquakes occur along a conjugate fault system. Multiple earthquakes occurring on conjugate fault systems, though rarely ruptured in a single event, have been observed in California from the Transverse ranges to Mexico (Nicholson *et al.,* 1986). Two notable examples of conjugate faulting are the Superstition Hills–Elmore Ranch earthquakes of 1987 (Hanks and Allen, 1989) and the Landers–Big Bear events of 1992 (Jones *et al.,* 1995). Surface geologic mapping has shown pervasive conjugate faulting in the Coso region (Roquemore, 1980). The Coso earthquakes discussed in this article are distinct because, although they occur along conjugate faults, they are temporally separated by an extended interevent gap. Compared to the above-mentioned examples of conjugate faulting in California, where mainshocks occurred within hours of one another, we observe a time gap of more than 16 months at Coso.

Stress Transfer between the 1996 and the 1998 Sequences

We compute the static stress field produced by the mainshock in 1996, Eq96, given the appropriate mechanism and location (Table 1). We then resolve those stresses onto the direction in which the background stress will interact with the fault that produces the 1998 events. This allows us to quantify the effect of Eq96 in changing the failure stress on faults parallel to the 1998 events. The procedure is similar to the stress step modeling described before with the primary difference being that we do not assume optimally oriented planes in this case. Instead, we assume that all faults are parallel to the one causing the 1998 events. We find that the Eq96 increases the stress in the fault causing the 1998 events by 0.15 MPa, suggesting that the 1996 event trigerred the 1998 earthquakes. Considering a 3.0 MPa stress drop for an earthquake of similar size as of Eq98, this suggests a clock-advance of ≈5% of the interevent time or less than 7 yr in our case.

Conclusions

The Coso earthquakes of 1996 and 1998 occurred on a conjugate fault system consisting of two, previously unknown, northwest-striking right-lateral and northeast-striking left-lateral faults, respectively. Both the faults are clearly delineated by the source mechanism of the mainshocks and the hypocenter locations of the aftershocks. The mainshocks that initiated the sequences are located within 900 m of one another and represent the largest recorded events in the Coso region. The relocated hypocenters suggest that both of these mainshocks occurred at the bottom of their respective rupture surfaces at depths of ≈9 km. While aftershocks in 1996 progress in time along the same direction, those in 1998 reverse trend after the occurrence of a large aftershock. A change in direction can be related to the presence of a fault that crosscuts the aftershock sequence. There are significant differences in the sizes of the aftershocks, *b*-values and temporal decay rates (as given by the *p* values) between the 1996 and 1998 sequences. The higher *p* value suggests that the earthquakes in 1998 occurred in a region of higher tectonic activity and higher heat flow than those in 1996. The earthquakes in 1998 are analyzed to obtain estimates of stress step and rate. We can infer that these earthquakes produced significant loading of the geothermal field. We estimate that the repeat cycle of earthquakes in the northeast-trending fault is approximately 135 years.

Acknowledgments

This research was supported by Grant N68936-97-C-0001 from the Naval Air Warfare Center. We thank the Navy Geothermal Program for providing the data. We are grateful to Doug Dreger of UC, Berkeley, for providing source mechanisms of the larger earthquakes. We thank associate editor Diane Doser, Scott Davis, and an anonymous reviewer for their comments that helped improve the article. Help from Adam Kosloff and Dionne Vink in analyzing the waveform data is appreciated. Kenji Obata's timely help in editing noisy data is acknowledged. Suggestions from Frank Monastero (Geothermal Program Office) have improved the manuscript. Gross thanks NSF Grant EAR-9628458 for partial support of this research.

References

Akaike, H. (1974). A new look at the statistical model identification, *IEEE Trans. Autom. Control* **AC-19,** 716–723.

Alvarez, M. G. (1992). The seismotectonics of the southern Coso Range observed with a new borehole seismographic network, *Master's Dissertation,* Duke University.

Anderson, J. G., J. N. Brune, J. Louie, Y. Zeng, M. Savage, G. Yu, Q. Chen, and D. dePolo (1994). Seismicity in the western Great Basin apparently triggered by the Landers, California, earthquake, 28 June, 1992, *Bull. Seism. Soc. Am.* **84,** 863–891.

Bodin, P. and J. Gomberg (1994). Triggered seismicity and deformation between the Landers, California, and Little Skull Mountain, Nevada, earthquakes, *Bull. Seism. Soc. Am.* **84,** 835–843.

Combs, J. and Y. Rotstein (1976). Microseismic studies of the Coso geothermal area, China Lake, California, in *Proc. of the 2nd United*

Nations Symposium on the Development and Use of Geothermal Resources 2, 909–916.

Creamer, F. H. (1994). The relation between temperature and earthquake aftershock decay for aftershock sequences near Japan, *Ph.D. Dissertation,* University of Colorado at Boulder.

Dieterich, J. H. (1986). A model for nucleation of earthquake slip, *Geophys. Monogr., Am. Geophys. Union 37,* 37–47.

Dieterich, J. H. (1994). A constitutive law for rate of earthquake production and its application to earthquake clustering, *J. Geophys. Res.* **99,** 2601–2618.

Duffield, W. A., C. R. Bacon, and G. B. Dalrymple (1980). 1996, Late cenozoic volcanism, geochronology and structure of the Coso Range, Inyo County, California, *J. Geophys. Res.* **85,** 2381–2404.

Feng, Q. and J. Lees (1998). Microseismicity, stress and fracture within the Coso geothermal field, *Phys. Earth Planet. Interiors* **289,** 221–238.

Gross, S. J. (1996). Aftershocks of nuclear explosions compared to natural aftershocks, *Bull. Seism. Soc. Am.* **86,** 1054–1060.

Gross, S. J. and R. Bürgmann (1998). Rate and state of background stress estimated from the aftershocks of the Loma Prieta, California, earthquake, *J. Geophys. Res.* **103,** 4915–4927.

Gross, S. J. and C. Kisslinger (1994). Tests of models of aftershock decay, *Bull. Seism. Soc. Am.* **84,** 1571–1579.

Gross, S. J. and C. Kisslinger (1997). Estimating tectonic stress rate and state with Landers aftershocks, *J. Geophys. Res.* **102,** 7603–7612.

Hanks, T. C. and C. R. Allen (1989). The Elmore Ranch and Superstition Hills earthquakes of 24 November 1987: introduction to the special issue, *Bull. Seism. Soc. Am.* **79,** 231–238.

Hauksson, E. (1994). State of stress from focal mechanisms before and after the Landers earthquake sequence, *Bull. Seism. Soc. Am.* **84,** 917–934.

Hauksson, E., K. Hutton, H. Kanamori, L. Jones, J. Mori, S. Hough, and G. Roquemore (1995). Preliminary report on the 1995 Ridgecrest earthquake sequence in eastern California, *Seism. Res. Lett.* **66,** 54–60.

Hill, D. P., P. A. Reasenberg, A. Michael, W. J. Arabasz, G. Beroza, D. Brumbaugh, J. Brune, R. Castro, S. Davis, D. dePolo, W. Ellsworth, J. Gomberg, S. Harmsen, L. House, S. M. Jackson, M. J. Johnston, L. Jones, R. Keller, S. Malone, L. Munguia, S. Nava, J. Pechmann, A. Sanford, R. W. Simpson, R. B. Smith, M. Clark, M. Stickney, A. Vidal, S. Walter, V. Wong, and J. Zollweg (1993). Seismicity remotely triggered by the magnitude 7.3 Landers, California, earthquake, *Science* **260,** 1617–1623.

Jennings, C. W. (1994). Fault activity map of California and adjacent areas with location and ages of recent volcanic eruptions, *California geologic data map series, Map No. 6,* California Division of Mines and Geology.

Jones, L., J. Mori, and E. Hauksson (1995). The Landers earthquake: preliminary instrumental results, *Earthquakes Volcanoes* **23,** 200–208.

King, G. C., R. S. Stein, and J. Lin (1994). Static stress changes and the triggering of earthquakes, *Bull. Seism. Soc. Am.* **84,** 935–953.

Kisslinger, C. (1993). The stretched exponential function as an alternative model for aftershock decay rate, *J. Geophys. Res.* **98,** 1913–1922.

Kisslinger, C. (1996). Aftershocks and fault-zone properties, *Adv. Geophys.* **38,** 1–36.

Kisslinger, C. and L. M. Jones (1991). Properties of aftershock sequences in southern California, *J. Geophys. Res.* **96,** 11947–11958.

Lees, J. M. (1998). Multiplet analysis at Coso geothermal, *Bull. Seism. Soc. Am.* **88,** 1127–1143.

Malin, P. (1994). The seismology of extensional hydrothermal systems, *Geothermal Resources Council Trans.* **18,** 17–22.

Mikumo, T. and T. Miyatake (1979). Earthquake sequences on a frictional fault model with non-uniform strengths and relaxation times, *Geophys. J. R. Astr. Soc.* **54,** 417–438.

Mogi, K. (1967). Earthquakes and fractures, *Tectonophysics* **5,** 35–55.

Nicholson, C., L. Seeber, P. Williams, and L. R. Sykes (1986). Seismic evidence for conjugate slip and block rotation within the San Andreas fault system, southern California, *Tectonics* **5,** 629–648.

Reasenberg, P. and L. M. Jones (1989). Earthquake hazard after a mainshock in California, *Science* **243,** 1173–1176.

Reasenberg, P. and R. W. Simpson (1992). Response of regional seismicity to the static stress change produced by the Loma Prieta earthquake, *Science* **255,** 1687–1690.

Roquemore, G. (1980). Structure, tectonics, and stress field of the Coso Range, Inyo County, California, *J. Geophys. Res.* **85,** 2434–2440.

Roquemore, G. (1987). The microseismicity of the shallow geothermal reservoir in the Coso Range, California, *Seism. Res. Lett.* **58,** 29.

Scholz, C. H. (1990). *The Mechanics of Earthquakes and Faulting,* Cambridge University Press, Cambridge.

Thomas, G. C., R. S. Crosson, D. L. Carver, and T. S. Yelin (1996). The 25 March 1993 Scotts Mills, Oregon, earthquake and aftershock sequence; spatial distribution, focal mechanisms, and the Mount Angel Fault, *Bull. Seism. Soc. Am.* **86,** 925–935.

Utsu, T. (1961). A statistical study on the occurrence of aftershocks, *Geophys. Mag.* **30,** 521–605.

Wald, L. A., J. Mori, and D. J. Wald (1997). The 1996 southern California network bulletin, *Seism. Res. Lett.* **68,** 923–929.

Walter, A. W. and C. S. Weaver (1980). Seismicity of the Coso Range, *J. Geophys. Res.* **85,** 2441–2458 (1997).

Whitmarsh, R. S. (1998). Structural development of the Coso Range and adjacent areas of east–central California, *Ph.D. Dissertation,* University of Kansas, Lawrence.

Wu, H. and J. Lees (1996). Attenuation structure of Coso geothermal area, California, from wave pulse widths, *Bull. Seism. Soc. Am.* **86,** 1574–1590.

Wu, H. and J. Lees (1999). Three-dimensional *P*- and *S*-wave velocity structures of Coso geothermal area, California, from microseismic traveltime data, *J. Geophys. Res.* (in press).

Department of Geology and Geophysics
Yale University
210 Whitney Avenue
New Haven, Connecticut 06511
E-mail: joydeep@hess.geology.yale.edu
(J. B., J. L.)

CIRES
University of Colorado
Boulder, Colorado
(S. G.)

Naval Geothermal Program
NAWS
Chinalake, California
(M. H.)

Manuscript received 25 June 1998.